56th CIRP Conference on Manufacturing Systems, CIRP CMS '23, South Africa

Methodology for the characterization and understanding of longitudinal wrinkling during calendering of lithium-ion and sodium-ion battery electrodes

Ann-Kathrin Wurba[a,*], Julian Klemens[b], Dominik Mayer[a], Constantin Reusch[a], Lennart Altmann[a], Olatz Leonet[c], J. Alberto Blázquez[c], Iker Boyano[c], Elixabete Ayerbe[c], Philip Scharfer[b], Wilhelm Schabel[b], Jürgen Fleischer[a]

[a]*Institute of Production Science (wbk), Karlsruhe Institute of Technology (KIT), Kaiserstr. 12, 76131 Karlsruhe, Germany*
[b]*Thin Film Technology (TFT), Material Research Center for Energy Systems (MZE), Karlsruhe Institute of Technology, Hermann-von-Helmholtz-Platz 1, 76344 Eggenstein-Leopoldshafen, Germany*
[c]*CIDETEC, Basque Research and Technology Alliance (BRTA), Pº Miramón, 196, 20014 Donostia-San Sebastián, Spain*

* Corresponding author. Tel.: +49 1523 9502617; fax: +49 721 608 45005. *E-mail address:* ann-kathrin.wurba@kit.edu

Abstract

The manufacturing of lithium-ion battery (LIB) cells is following a complex process chain in which the individual process steps influence the subsequent ones. Meanwhile, increasing requirements especially concerning the battery performance, sustainability and costs are forcing the development of innovative battery materials, production technologies and battery designs. The calendering process directly affects the volumetric energy density of an electrode and therefore of a battery cell. Calendering is still challenging as it causes high stresses in the electrode that lead to defects and thus increased rejection rates. The interaction between electrode material and process as well as the formation of defects is still not fully understood, especially when new material systems are used. In this context, the sodium-ion battery (SIB) is one post-lithium battery system that is a promising option to overcome the limitations of conventional LIBs. Therefore, this paper presents a first material and machine independent methodology to describe and understand the defect type longitudinal wrinkle, which mostly appears at the uncoated current collector edge of an electrode and in running direction. The aim is to systematically characterize the longitudinal wrinkles according to their geometry. The automatic data acquisition is carried out with a laser triangulation system and a 3D scanning system. The geometry values are calculated from the raw data and correlated to selected process parameters. The methodology is applicable regardless of the material as shown by exemplary results of NMC811 cathodes for LIB and hard carbon anodes for SIB. By using two different pilot calenders it is shown, that the data acquisition can be carried out independently of the machine. The presented methodology contributes to finding solutions for the avoidance of longitudinal wrinkling in any battery electrode and therefore to reducing the rejection rate.

Keywords: lithium-ion battery, sodium-ion battery, electrode manufacturing, calendering, longitudinal wrinkling

1. Introduction

Currently the lithium-ion battery (LIB) is an established technology for energy storage for a broad field of applications.

Due to rapidly improving technologies in these fields, the demand for better performing, safer, more sustainable and cheaper batteries is also increasing. [1–3] There are several approaches to overcome these limitations such as optimization

of the material [4], production process [5] and new battery technologies like post-lithium systems [1]. A promising battery technology besides the LIB is the sodium-ion battery (SIB), which is about to become widely commercialized [1]. The SIB is a so-called drop-in technology as the material and production process is roughly like the lithium-ion technology. But there are still some differences while a standard manufacturing route for different material properties and new material systems is not established. [6,7]

Understanding the material behavior is necessary to improve the manufacturing of electrodes and thus reduce rejection rates [8]. The process chain is complex and each process step is determining the following one. Each production step must be adapted to the materials requirements to avoid damages in the following processes. [9] Calendering is crucial to set the volumetric energy density of the electrode, which is directly related to the battery's performance. [8,10,11] The porous electrode coating material is compressed in a rolling process under high load [11]. As a result, the coating is densified and mechanical stresses are introduced that lead to defects. The defects negatively affect the material quality as well as the productivity. [8,12] There are several different calendering defects that influence the web handling. Deformations over the entire electrode width like corrugations in and orthogonal to the running direction as well as bulge-shapes are observed. At high compaction rates and high web tensions foil embossing appears. This defect consists of small wrinkles that occur at a certain angle to the running direction on the uncoated substrate. Furthermore, it has been observed that a high compaction stiffens the electrode. [8,12,13] There are already approaches for recording the deformations of calendered electrodes with a laser triangulation system [14] and a 3D-scanner [12].

This paper focusses on the description and the understanding of the formation of the defect pattern longitudinal wrinkling that is well-known among electrode manufacturers as it can cause web tears. Nevertheless, scientifically it has been only described for other web processing industries like the metal strip manufacturing where they are defined as plastic creases occurring at deflection rollers and in parallel to the running direction. The high web tension in general leads to buckling of the metal strip. Simulations showed that additional stresses are caused by friction during motion of the web, which leads to exceeding the critical tension to form a plastic crease. [15,16]

On electrodes longitudinal wrinkles are similar as they occur in parallel to the running direction after a strong compaction when hitting the first deflection roller with a high web tension. A methodology is developed to characterize the geometry of longitudinal wrinkles in calendered electrodes for different materials depending on the process parameters. Data is collected experimentally during calendering using a laser triangulation sensor and a 3D scanning system. Calendering experiments are performed on two calenders with two electrode materials to investigate the applicability of the presented methodology.

2. Experimental

In this section the calenders, electrode materials, sensors and experimental settings are introduced.

2.1. Calender systems

The calender of the Karlsruhe Institute of Technology (KIT) is a GKL 500 MS (Saueressig Group). The calender rollers have a diameter of 700 mm and a width of 500 mm and are able to apply a maximum line load of about 2000 N·mm^{-1} on the electrode. The rollers can be tempered up to 90 °C, with room temperature as lower limit. The web tension can be set individually for the rewinder, unwinder and the separate tension unit in a range of 1 N to 250 N. The web speed is adjustable between 1 m·min^{-1} and 30 m·min^{-1}. [17] A schematic of the calender is shown in Fig. 1 in the foreground.

In the background of Fig. 1 the schematic of the calender LDHY400-N45 (Xingtai Naknor Technology Co., Ltd) installed at CIDETEC is shown. The upper deflection roller of the tension unit is located at a lower level than the calender rollers, so a supporting deflection roller is installed. The diameters of the rollers are 400 mm and the widths are 450 mm with a linear pressure of 2400 – 3700 N·mm^{-1}. The applied resulting line load is not recordable. Two deflection rollers can be heated up to 180 °C to preheat the electrode before entering the calender rollers. The web tension cannot be set to a specific value. During operation a proportion of the maximum torque is applied. [18]

2.2. Electrode materials

The coating of both electrodes is placed symmetrically in the center and on both sides of a 15 µm aluminum foil. Further properties of the dry electrode are displayed in Table 1. The NMC811 cathode contains 94.0 wt-% active material, 3.0 wt-% carbon black and 3.0 wt-% polyvinylidene fluoride (PVDF) and was manufactured by Enertech International.

The HC anode was manufactured at CIDETEC. The dry electrode contains 93.0 wt-% of HC (BHC-400 from Shandong Gelon LIB Co., Ltd), 1.4 wt-% carbon black, 1.87 wt-% carboxymethyl cellulose (CMC), and 3.73 wt-% styrene-butadiene rubber (SBR). The coating was performed on the pilot coating machine BC39 from Coatema Coating Machinery GmbH.

Table 1. Properties of the dry uncalendered electrodes

	Mass loading / mg·cm^{-3}	Coating width / mm	Substrate width / mm	Density / g·cm^{-3}	Coating thickness / µm
NMC811	41.60	155	215	2.17	188.0
HC	19.61	155	250	0.88	223.5

2.3. Sensor systems

As shown in Fig. 1 the data acquisition systems are located after the calender rollers at the tension unit. The laser triangulation sensor LJ-V7060B (Keyence Deutschland GmbH) is permanently installed above the electrode. Within one measurement procedure 10000 profiles were recorded with a frequency of 500 Hz and a width of 15 mm. [19]

The optical 3D scanner ATOS Core 135 (Carl Zeiss GOM Metrology GmbH) is built with two cameras and a projector

that emits narrowband blue LED light. The system is mounted on a movable tripod to generate images from different angles within a measuring range of 135 mm × 100 mm. [20]
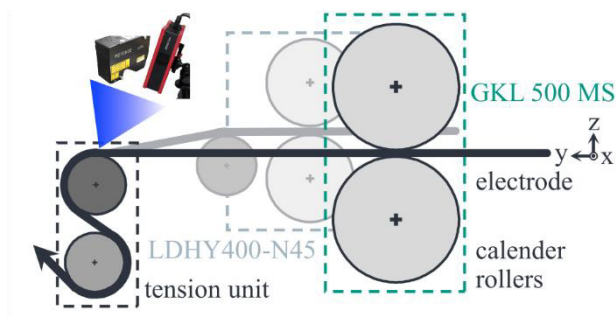

Fig. 1. Experimental setup with the relevant parts of the calendering machines GKL 500 MS (foreground) and LDHY400-N45 (background) with the sensor systems ATOS Core 135 and LJ-V7060B

2.4. Calendering experiments

The investigated process parameters are the web tension, the temperature and the density of the calendered electrode. The density is calculated from the mass loading of the coating divided by the coating thickness. All experiments were performed with a web speed of 1 m·min⁻¹.

The exemplary investigations on the NMC811 cathodes were conducted on the GKL 500 MS at KIT with the laser and the 3D scanning system. The parameters for the experiments NMC_A and NMC_B at different densities are shown in Table 2. The web tensions were 110 N for the tension unit and 60 N each for unwinder and rewinder.

The HC anode was calendered on the LDHY400-N45 at CIDETEC under the conditions displayed in Table 2. Calendering of HC_A was done with proportions of the torque of 20 % for the unwinder and 33 % for the rewinder. For HC_B the proportions of the torque were increased to 25 % for the unwinder and 38 % for the rewinder as no longitudinal wrinkle was observed at lower web tensions and a therefore looser web. As shown in Table 2, the HC electrodes were calendered to the same thickness resp. density at two temperatures. The data acquisition was exclusively done with the laser system.

Table 2. Parameter setting for calendering experiments with NMC811 and HC to examine longitudinal wrinkles

	Density / g·cm⁻³	Coating thickness / μm	Temperature / °C
NMC_A	2.84	145.5	30
NMC_B	3.34	124.0	30
HC_A	1.09	177.8	100
HC_B	1.08	176.3	25

3. Characterization of longitudinal wrinkling

3.1. General geometrical description

Longitudinal wrinkles are arch shaped irreversible plastic deformations in both uncoated current collectors. In both electrode materials a longitudinal wrinkle was formed. Fig. 2a)

shows a photograph and b) a 3D scan colored according to the height of an NMC811 cathode that is spread over the first deflection roller. The running direction is in y-direction. In Fig. 2b) the white box marks the potential area for the formation of longitudinal wrinkles. The profile cut in the 3D scan is needed for the evaluation of the geometry and is described in section 3.2.
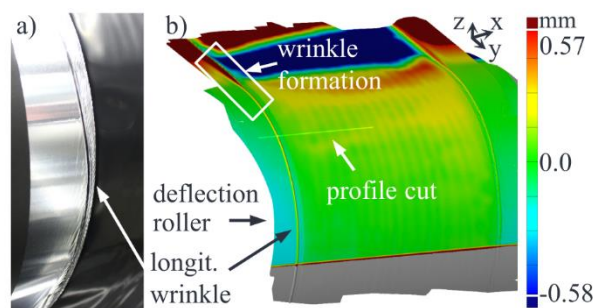

Fig. 2. Wrapped cathode with longit. wrinkle, a) photograph, b) 3D scan

Fig. 3 shows a schematic profile of a longitudinal wrinkle with the points needed to calculate its geometry values height (h), width (w) and distance (d) to the coating edge.

In this case, the coated part is located on the left side and the uncoated current collector (substrate) is shown on the right. The point C marks the end of the coated part. The points W_1 and W_2 represent the left and right limitation of the longitudinal wrinkle. The width of the longitudinal wrinkle is calculated from the difference between $x(W_2)$ and $x(W_1)$ as shown below.

$$w = x(W_2) - x(W_1) \tag{1}$$

The height is defined as the distance between the tip of the longitudinal wrinkle $z(W_t)$ and the limitation of the longitudinal wrinkle which is on the side without the coating, as there is no interference with foil embossing. Referring to Fig. 3 the correct limitation is $z(W_2)$.

$$h = z(W_t) - z(W_2) \tag{2}$$

The distance between the coating and the longitudinal wrinkle is defined as difference between the coating edge $x(C)$ and the tip point of the wrinkle $x(W_t)$.
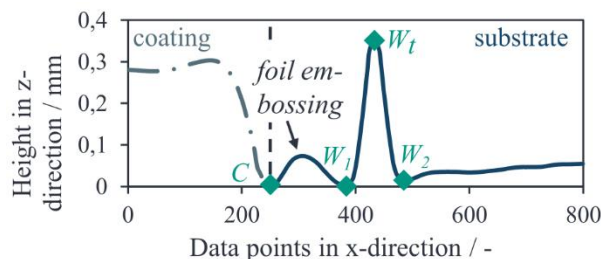
$$d = x(W_t) - x(C) \tag{3}$$

Fig. 3. Geometric shape of a longitudinal wrinkle shown as profile of the electrode

3.2. Data acquisition and processing

In the following the methodology to investigate the longitudinal wrinkles for different machines and materials is described. In the first step, the investigated process parameters roll temperature, web tension and the density of the electrode have to be defined. Afterwards the calendering is performed. As soon as the calendered part hits the first deflection roller, the data acquisition with the laser sensor starts within the software LJ-X Navigator (Keyence Deutschland GmbH). For the data processing, the laser data is exported as a CSV file.

After the collection of the laser data, the calendering process is stopped, as the data acquisition with the ATOS Core 135 requires an unmoving electrode. The deflection roller with the wrapped electrode is scanned within the software GOM Inspect (Carl Zeiss GOM Metrology GmbH). As the uncoated current collector causes interfering reflections, it is sprayed with a standard black aerosol spray before taking the images. Furthermore, reference dots are applied irregularly on the electrode to process the single images to one 3D mesh afterwards. This 3D mesh of the wrapped electrode surface from the 3D scanning is compared to a CAD model of an ideally even wrapped electrode and the height differences are calculated automatically in GOM Inspect. Approximately 15 to 20 profiles with valid data transverse to the running direction are selected by the user and the height differences are also exported to a CSV file.

The CSV files from the laser and the 3D scanning system are then processed within two Matlab tools, one for each data acquisition type. Fig. 4 shows the data processing within Matlab as an overview. The core process for the calculation of the geometry parameters is identical for the laser profiles and the profiles of the 3D scan. The core process is therefore described only once. The data processing is challenging due to measurement errors caused by reflections and defects like foil embossing (see Fig. 3). Reflection errors occur as nearly vertical peaks in the laser profiles and are detected by a pre-filter described below. The corresponding profiles are not used for the calculation of the geometry parameters. In the 3D scan these reflection errors appear as missing data in the profiles and are excluded by the user in advance. The filter for the laser data utilizes, that the slopes of the peaks are higher compared to slopes from the longitudinal wrinkle or the coating edge. Noise in the profiles caused by the uneven electrode is smoothed using the Matlab moving average filter. From the second derivatives of all smoothed profiles the maximum difference of the value range is extracted and plotted in a histogram. The user selects the threshold that separates natural from unnatural high slopes that indicate a reflection error. Further processing is done with the unsmoothed profiles that are free from errors.
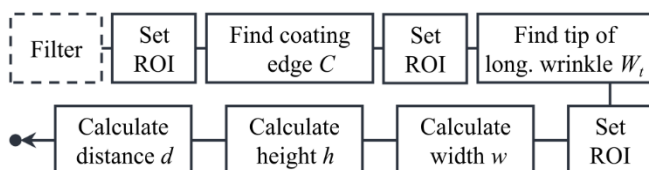

Fig. 4. Flow chart for the data processing via the Matlab codes for the laser and 3D scanning data

The user selects the region of interest (ROI) in a 2D meshplot that contains a longitudinal wrinkle by choosing start and end points where the coating edge C is assumed to be located. A straight line is created from which the algorithm detects the next local minimum in the surrounding of the assumed edge line. If the algorithm is unable to correctly detect the local minima, because of disturbances caused by calendering defects, the user has the choice to set the pre-selected line as the coating edge or to reset the ROI. Afterwards, the user selects the assumed tip line W_t of the longitudinal wrinkle from which the next local maximum is searched. Then the user specifies the ROI for the width limitation line of the longitudinal wrinkle W_1 and W_2 from an example profile plot. The points are the next local minima in the search area to the left and right of the tip line as shown in Fig. 3. The width is then calculated from the two limitation points using equation (1). Afterwards the height is calculated for each profile with the tip points and the associated width limitation point according to equation (2). The distance of the wrinkle is then calculated using equation (3).

All geometry values are calculated for each profile from the laser data and the 3D scan and transferred to average values that represent the longitudinal wrinkle. Non-parallel longitudinal wrinkles thus show a higher standard deviation for the distance than parallel ones. The final resulting geometry values for the longitudinal wrinkle correspond to the average of the 3D scan and the laser data.

4. Results and discussion

Fig. 5 shows an exemplary processed data set from the experiment HC_A. The 3D mesh plot corresponds to the schematic profile view shown in Fig. 3. The coating can be seen on the left side. The outer edge of the coating (transition to the substrate) is marked in white at $x \approx 5\ mm$. Foil embossing can be observed between the outer coating edge and the longitudinal wrinkle. The left and right width limitation points of the longitudinal wrinkle are marked in red, while the tip points are represented in black. On the right side the rest of the uncoated current collector is displayed.
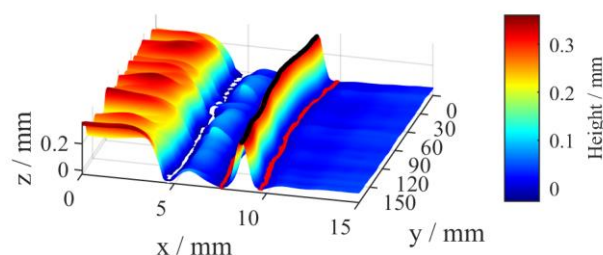

Fig. 5. 3D mesh plot of the processed laser data of HC_A

In the following, the results of the calendering experiments are discussed.

The respective average geometry values for NMC811 with the two different densities of $2.84\ \mathrm{g \cdot cm^{-3}}$ (NMC_A) and $3.34\ \mathrm{g \cdot cm^{-3}}$ (NMC_B) are compared in Fig. 6. They are calculated individually from the 3D scan and the laser measurement of a single calendering process.

The differences do not show any regularities and apart from the distance for the NMC_B the differences are small. Thus, the measurements are assumed to be realistic. Major deviations, such as for the distance are attributed to calendering defects that interfere with the evaluation. It also must be considered that both measurement systems do not record the exact same section of the longitudinal wrinkle, as the 3D scan is started after the laser measurement.
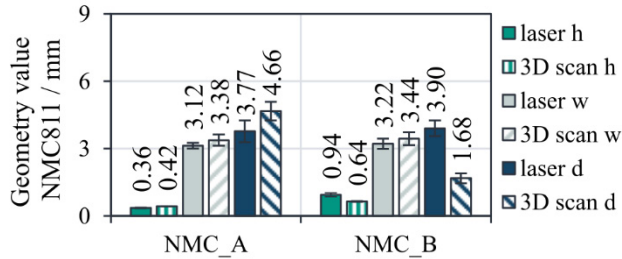

Fig. 6. Height (h), width (w) and distance (d) of longitudinal wrinkles for NMC811 separated by measurement methods laser and 3D scan

Fig. 7. shows the resulting average geometry values of the formed longitudinal wrinkles during calendering for NMC_A and NMC_B. The average height increases with increasing density. Due to the high standard deviation of the average distance, it is not obvious whether it decreases with increasing density. The average width is not influenced by the density. These preliminary results as well as earlier investigations performed at wbk-KIT indicate that the electrode deforms according to the high stresses during calendering [12]. All types of deformation described in section 1 contribute to an uneven electrode that is pulled over the deflection roller with a high web tension. The electrode is pressed on the deflection roller and is not free to compensate for the unevenness. The resulting compensation is therefore a wrinkle. A higher density leads to higher stresses in the electrode and probably to larger deformations. It is assumed that greater deformations need greater compensation which leads to higher longitudinal wrinkles at a constant width.
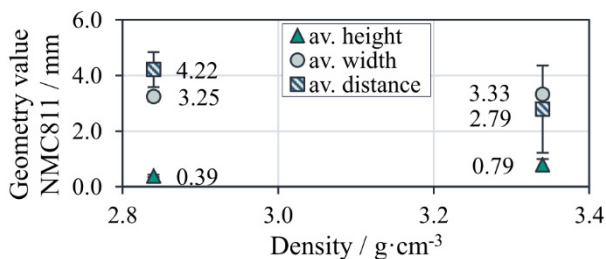

Fig. 7. Height, width and distance of longitudinal wrinkles for NMC811

Calendering of the HC anodes at 25 °C and 100 °C preheating temperature leads to the results from the laser data of one calendering process shown in Fig. 8.

Temperature does not have an influence on the average height as well as the average width of the longitudinal wrinkle. The average distance decreases when increasing the preheating temperature. An increasing temperature can increase the elasticity of the binder of anodes and cathodes and therefore decrease the line load effort for compaction. [21,22] As the electrode is already cold when it hits the deflection roller, no direct influence of an increased elasticity can be seen. For further assessment of the influence of the temperature the mechanical properties as well as the level of deformation after calendering should be regarded. Considering that the average web tension between unwinder and rewinder was higher for the experiment HC_B at 25 °C than for HC_A at 100 °C, this diagram also shows that the web tension has no influence on the average height and width of the longitudinal wrinkle, but on the average distance. This experiment confirms that, in general, a certain critical web tension is needed for the formation of longitudinal wrinkles, as also described in [16]. Nevertheless, further investigation is required to determine whether the temperature has an influence on the critical web tension. With this small number of experiments and no absolute values for the web tension, no definitive statement can be made about the cause and effect relationships.
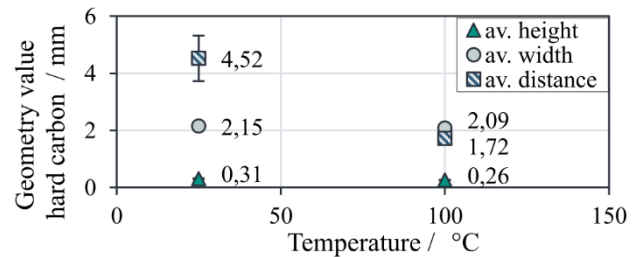

Fig. 8. Height, width and distance of longitudinal wrinkles for HC

5. Summary and outlook

Comparing the results with two different electrode materials and two different calenders, the data sets are in the same range of values. In both cases the average width was not influenced while the temperature, web tension and density seem to have an influence on the average height and distance.

It has been demonstrated that data acquisition with the laser system can be used with different calendering machines. However, the 3D scanning system was only tested at the calender GKL 500 MS at KIT. On both electrode materials longitudinal wrinkles were detected. The process parameters roll temperature, web tension and electrode density were recorded and correlated to the wrinkle parameters.

As this data set is limited to a small number of experiments, a systematic design of experiments is planned to point out the influence of the process parameters web tension, roll temperature and electrode density on the longitudinal wrinkling. Furthermore, the line load can be considered as a parameter that significantly influences the density [12]. The length of the longitudinal wrinkle was not yet recorded and is part of future investigations. For a deeper understanding of the formation of the longitudinal wrinkling the mechanical behavior and characteristic values such as the bending stiffness and Young's modulus of the electrode during and after calendering should be investigated in detail. An insight into the mechanisms of the compaction behavior is possible by measuring the resulting strains in the coating as proposed in [12]. Furthermore, an evaluation of the corrugations gives information on the extent of unevenness which seem to favor

the formation of longitudinal wrinkles. Different electrode materials should be compared while setting the same process parameters to determine the material's impact on longitudinal wrinkling.

These investigations contribute to develop an additional device that supports the guiding of the electrode web by applying additional transverse tensile forces to reduce the longitudinal wrinkling. This development will be part of future work. All in all, this work is a first step to minimize the rejection rate due to calendering defects.

Acknowledgements

References

[1] H. Liu, M. Baumann, X. Dou, J. Klemens, L. Schneider, A.-K. Wurba, M. Häringer, P. Scharfer, H. Ehrenberg, W. Schabel, J. Fleischer, N. von der Aßen, M. Weil, Tracing the technology development and trends of hard carbon anode materials - A market and patent analysis, Journal of Energy Storage 56 (2022) 105964. https://doi.org/10.1016/j.est.2022.105964.

[2] A. Kwade, W. Haselrieder, R. Leithoff, A. Modlinger, F. Dietrich, K. Droeder, Current status and challenges for automotive battery production technologies, Nat Energy 3 (2018) 290–300. https://doi.org/10.1038/s41560-018-0130-3.

[3] C. Daniel, Materials and processing for lithium-ion batteries, JOM 60 (2008) 43–48. https://doi.org/10.1007/s11837-008-0116-x.

[4] J. Klemens, L. Schneider, E.C. Herbst, N. Bohn, M. Müller, W. Bauer, P. Scharfer, W. Schabel, Drying of NCM Cathode Electrodes with Porous, Nanostructured Particles Versus Compact Solid Particles: Comparative Study of Binder Migration as a Function of Drying Conditions, Energy Tech 10 (2022) 2100985. https://doi.org/10.1002/ente.202100985.

[5] K. Husseini, N. Schmidgruber, S. Henschel, D. Mayer, J. Fleischer, Model‐Based Optimization of Web Tension Control for the Flexible Cell Stack Assembly of Lithium‐Ion Battery Cells, Energy Tech (2022) 2200679. https://doi.org/10.1002/ente.202200679.

[6] F. Duffner, N. Kronemeyer, J. Tübke, J. Leker, M. Winter, R. Schmuch, Post-lithium-ion battery cell production and its compatibility with lithium-ion cell production infrastructure, Nat Energy (2021). https://doi.org/10.1038/s41560-020-00748-8.

[7] J. Hofmann, A.-K. Wurba, B. Bold, S. Maliha, P. Schollmeyer, J. Fleischer, J. Klemens, P. Scharfer, W. Schabel, Investigation of

[8] T. Günther, D. Schreiner, A. Metkar, C. Meyer, A. Kwade, G. Reinhart, Classification of Calendering‐Induced Electrode Defects and Their Influence on Subsequent Processes of Lithium‐Ion Battery Production, Energy Technol. 8 (2020) 1900026. https://doi.org/10.1002/ente.201900026.

[9] M. Thomitzek, O. Schmidt, F. Röder, U. Krewer, C. Herrmann, S. Thiede, Simulating Process-Product Interdependencies in Battery Production Systems, Procedia CIRP 72 (2018) 346–351. https://doi.org/10.1016/j.procir.2018.03.056.

[10] W. Haselrieder, S. Ivanov, D.K. Christen, H. Bockholt, A. Kwade, Impact of the Calendering Process on the Interfacial Structure and the Related Electrochemical Performance of Secondary Lithium-Ion Batteries, ECS Trans. 50 (2013) 59–70. https://doi.org/10.1149/05026.0059ecst.

[11] C. Meyer, H. Bockholt, W. Haselrieder, A. Kwade, Characterization of the calendering process for compaction of electrodes for lithium-ion batteries, Journal of Materials Processing Technology 249 (2017) 172–178. https://doi.org/10.1016/j.jmatprotec.2017.05.031.

[12] D. Mayer, A.-K. Wurba, B. Bold, J. Bernecker, A. Smith, J. Fleischer, Investigation of the Mechanical Behavior of Electrodes after Calendering and Its Influence on Singulation and Cell Performance, 2021.

[13] B. Bold, J. Fleischer, Kalandrieren von Elektroden für Li-Ionen-Batterien, ZWF 113 (2018) 571–575. https://doi.org/10.3139/104.111968.

[14] A. Mayr, D. Schreiner, B. Stumper, R. Daub, In-line Sensor-based Process Control of the Calendering Process for Lithium-Ion Batteries, Procedia CIRP 107 (2022) 295–301. https://doi.org/10.1016/j.procir.2022.04.048.

[15] F.G. Rammerstorfer, Buckling of elastic structures under tensile loads, Acta Mech 229 (2018) 881–900. https://doi.org/10.1007/s00707-017-2006-1.

[16] N. Jacques, A. Elias, M. Potier-Ferry, H. Zahrouni, Buckling and wrinkling during strip conveying in processing lines, Journal of Materials Processing Technology 190 (2007) 33–40. https://doi.org/10.1016/j.jmatprotec.2007.03.117.

[17] SAUERESSIG GmbH + Co. KG, Betriebsanleitung GKL 500 MS, 2013.

[18] Xingtai Naknor Electrode Rolling Equipment Co., Ltd, Technical Appendix (Model: LDHY 400-N45), 2012.

[19] Keyence Deutschland, Datenblatt LJ-V7060 Messkopf, https://www.keyence.de/products/measure/laser-2d/lj-v/models/lj-v7060/, accessed 8 January 2023.

[20] GOM mbH, Atos Core: Benutzerhandbuch - Hardware, Braunschweig, 2013.

[21] N. Billot, T. Günther, D. Schreiner, R. Stahl, J. Kranner, M. Beyer, G. Reinhart, Investigation of the Adhesion Strength along the Electrode Manufacturing Process for Improved Lithium‐Ion Anodes, Energy Technol. 8 (2020) 1801136. https://doi.org/10.1002/ente.201801136.

[22] C. Meyer, M. Weyhe, W. Haselrieder, A. Kwade, Heated Calendering of Cathodes for Lithium‐Ion Batteries with Varied Carbon Black and Binder Contents, Energy Technol. 8 (2020) 1900175. https://doi.org/10.1002/ente.201900175.

Parameters Influencing the Producibility of Anodes for Sodium-Ion Battery Cells, in: B.-A. Behrens, A. Brosius, W. Hintze, S. Ihlenfeldt, J.P. Wulfsberg (Eds.), Production at the leading edge of technology, Springer Berlin Heidelberg, Berlin, Heidelberg, 2021, pp. 171–181.